REPORT DOCUMENTATION PAGE

AFRL-SR-AR-TR-02-

0232

1. AGENCY USE ONLY *(Leave blank)*	2. REPORT DATE	3. REPORT TYPE AND DATES COVERED
		01 Jan 98 to 31 Dec 00 FINAL

4. TITLE AND SUBTITLE
Physics and Modeling of Compound SemiConductor Devices with Semi-Insulating and Native-Oxide Layers

5. FUNDING NUMBERS
61102F
2305/BX

6. AUTHOR(S)
Dr. Grublin

7. PERFORMING ORGANIZATION NAME(S) AND ADDRESS(ES)
Scientific Research Assoc
PO Box 1058
50 Nye Road
Glastonbury CT 06033

8. PERFORMING ORGANIZATION REPORT NUMBER

9. SPONSORING/MONITORING AGENCY NAME(S) AND ADDRESS(ES)
AFOSR/NE
801 North Randolph Street Rm 732
Arlington, VA 22203-1977

10. SPONSORING/MONITORING AGENCY REPORT NUMBER
F49620-98-C-0001

11. SUPPLEMENTARY NOTES

12a. DISTRIBUTION AVAILABILITY STATEMENT
APPROVAL FOR PUBLIC RELEASED; DISTRIBUTION UNLIMITED

12b. DISTRIBUTION CODE

13. ABSTRACT *(Maximum 200 words)*

In looking at the literature the two primary sources for two-dimensional calculations that were found were Chin et. at [6]and Poncet [7]. Both of these investigators essentially solve the same set of governing equations. Chin solved a similar problem to that addressed above, but the computational domain was limited to the oxide only. No calculation was performed in either the virgin material or the mask. Poncet' s problem is somewhat different and he does solve the governing equations in two separate regions. However he does not solve the governing equations in the virgin material and in the masks. Thus neither of the investigators concerns themselves with the coupled interface problem between the oxide and virgin material that was attempted in our study. The SEX study in that sense is much more ambitious. It has demonstrated that the pedestal and the cap do have an influence on the physics of the computation and they can have a significant effect on the shape of the oxide sub-region.

20020816 066

14. SUBJECT TERMS			15. NUMBER OF PAGES
			16. PRICE CODE
17. SECURITY CLASSIFICATION OF REPORT	18. SECURITY CLASSIFICATION OF THIS PAGE	19. SECURITY CLASSIFICATION OF ABSTRACT	20. LIMITATION OF ABSTRACT
UNCLASSIFIED	UNCLASSIFIED	UNCLASSIFIED	UL

Scientific Research Associates, Inc.
P. O. Box 1058
Glastonbury, CT 06033
Tel: (860) 659-0333 Fax: (860) 633-0676

Final Report R02-9142-F

Physics and Modeling of Compound Semiconductors Devices with Semi-insulating and Native-Oxide Layers

Principal Investigator: Dr. H. L. Grubin
Email: hal@srassoc.com

Air Force Office of Scientific Research
Contract: F49620-98-C-0001

Reporting Period: 1 January 1998-31 December 2000

Physics and Modeling of Compound Semiconductor Devices with Semi-Insulating and Native-Oxide Layers

Table of Contents

Physics and Modeling of Compound Semiconductor Devices with Semi-Insulating and Native-Oxide Layers

Introduction

This final report summarizes the results of Scientific Research Associates, Inc. simulation of the lateral oxidation of AlAs based oxides.

The Physical Model

The oxidation model used here has been discussed in previous reports. Briefly, in the first reporting period, as a means of checking some of the equations we examined the standard Deal and Grove [1] model, a one dimensional elastic model for oxidation of films at least 300A thick. The model is one-dimensional. This model remains relevant today, although today's simulations allow for the presence of lateral stresses that can alter the shape of the interface.

Within the Deal and Grove model, for oxidation to occur three stages must occur: (i) the oxidizing species moves from the oxygen containing gas across the gas-oxide interface; (ii) the oxidizing species must move across the oxide region; and (iii) the oxidizing species reacts with the semiconductor at the oxide-semiconductor interface. Within the framework of this model there are two limiting situations of interest: The first is referred to as diffusion controlled where the rate of oxidation is limited by the availability of oxidant at the semiconductor-oxide interface. The second is referred to as concentration-reaction controlled where the oxidation rate is controlled by the concentration of oxidant at the semiconductor surface and by the rapidity with which the oxidation reaction can proceed. Ochiai, et al [2] in studying the lateral thermal oxidation of AlAs in water vapor in vertical cavity surface emitting laser structures observed: (i) At high temperatures and long oxidation times, diffusion across the oxide was the controlling mechanism; (ii) At low temperatures and short oxidation times, oxide growth was found to be reaction limited. These conclusions were based upon implementation of the rate equations developed in reference 1.

What is done experimentally? Two results illustrate. In [2] growth versus time was fit to the expression: $x_0^2 + ax_0 = bt$ In it was observed that for short oxidation times and thin oxide layers, this expression reduced to a linear growth law. At the pressures of ~ 1 atm and flow rates used in [2] the linear growth was considered to be reaction rate limited. This was confirmed by the observation that either doubling or reducing the N2 flow rate by half had no detectable influence on the growth rate, indicating saturation of the carrier gas. Alternatively, for long oxidation times and thicker oxides, or where oxidant diffusion across the oxide was the rate limiting mechanism, the oxidation followed a parabolic growth law. Very similar results were obtained by Naone and Caldren [3] where additionally the dependence of oxide growth on oxide thickness was also studied. Several observations were emphasized here: (i) The activation energy for the oxidation reaction was higher for the thinner layers; and (ii) the oxide tip of thicker layers was noticeably blunter than that of the thinner layers.

On the basis of the above results, as well as results of others it has become clear that for the AlAs oxidation model:

1. Two-dimensionality exists due to the difference in the diffusion coefficients of the oxide and that of the surrounding oxide. Additionally, the complex two-dimensionality is introduced because the oxidation front moves primarily in the horizontal direction, while stresses on the oxide are primarily in the vertical direction.

2. A viscous and/or visco-elastic model must be used.

To undertake this study we considered the computational region shown in figure 1. The region of interest (or computational domain) consists of the four specific subregions: (1) the oxide, (2) the pedestal, (3) the cap and (4) the virgin AlAs material. Initially the overall structure is assumed to be rectangular. As oxygen is passed over the virgin AlAs material an oxide layer develops and penetrates into the virgin material. Stresses will develop primarily between the pedestal, the cap, the oxide and the virgin AlAs layers thus distorting the overall structure into a non-rectangular shape.

We are interested in predicting the time-dependent development of both the shape of the structure and the penetration of the oxide layer into the virgin AlAs material. To do this and to determine how the overall geometry of the device is distorted in time, the governing system of partial differential equations that describe the physics must be developed. Boundary conditions on the various surfaces and interface conditions between the various sub-regions must be determined. Finally a strategy must be developed for solving the system of governing equations with appropriate boundary and interface conditions so that the physics can be predicted.

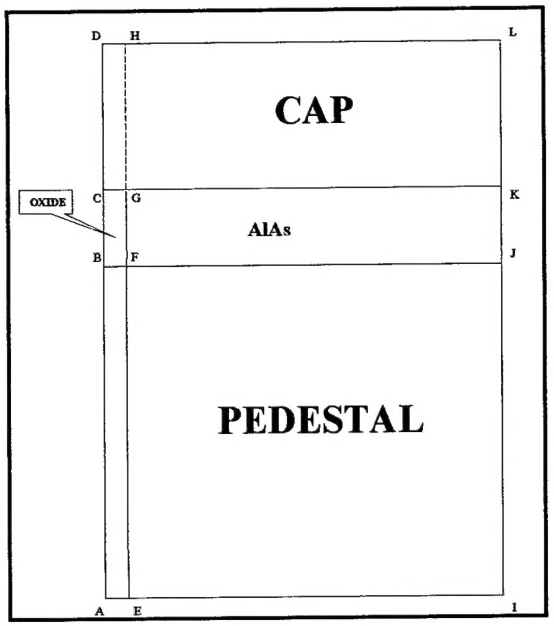

Figure 1. Initial Computational Region

The Governing Equations

For the structure of figure 1, Newton's second law and the basic principle of conservation of mass describes the physics of the system in all four sub-regions. The oxidation process is assumed occur at temperatures that are high enough for the stress-strain relationship to be that of a fully viscous fluid. Hence Newton's second law is described by the so-called Navier-Stokes system of partial differential equations. The compressibility of the oxide and the surrounding materials is very small so that the materials may be considered to be incompressible although the densities of the various materials may differ. Under these assumptions, the time dependent conservation of mass and the Navier-Stokes equations are expressed by the partial differential equation as

$$(1) \qquad \frac{\partial \rho}{\partial t} = \nabla \bullet \rho \vec{V}$$

and

$$(2) \qquad \frac{\partial \rho \vec{V}}{\partial t} = -\nabla P - \nabla \bullet \rho \vec{V}\vec{V} + \nabla \bullet \tau$$

Here ρ is the density, P is the pressure, τ is the stress tensor and $\vec{V}$ is the velocity vector consisting of the Cartesian components. The stress tensor, τ, is related to the velocity vector by the relationship

$$(3) \qquad \tau = \mu\left(\nabla \vec{V} + \nabla \vec{V}^{T}\right)$$

where μ is the viscosity of the material, and may, in general, be position dependent. The superscript T refers to the transpose.

The dynamics of the diffusion of the oxide concentration in the oxide layer is determined by the solution of the Laplace diffusion equation. Because of the physics of the situation the oxide is prevented from diffusing either into the pedestal or the cap. The governing equation takes the form

$$(4a) \qquad \rho \frac{\partial C}{\partial t} = \nabla \bullet D \nabla C$$

where C is the concentration of the oxide and D is the diffusion coefficient. Actually equation (4a) was modified in a manner suggested by Yoshikawa, et al [4].

$$(4b) \qquad \rho \frac{\partial C}{\partial t} = \nabla \bullet \left(D \nabla C - B\mathbf{S}C\right)$$

Here B represents the mobility of the diffusion material (the oxide) and **S** represents a stress tensor. The term $B\mathbf{S}C$ represents the surface interaction between the pedestal and cap with the oxide. It can easily be seen that the diffusion equation for the concentration is not coupled to either the conservation of mass or the Navier-Stokes equations. It will be shown that there is a coupling of the equations, but this is due to the interface conditions between the oxide layer and the virgin AlAs. In the case of lateral oxidation the inner stress comes mainly from the boundary plane to the upper and lower layers that sandwich the oxide layer.

The Boundary Conditions

Let us consider first the boundary conditions used with the conservation of mass and Navier-Stokes equations. This discussion is for two-dimensional cases but could easily be expanded to three dimensions. Since the pedestal is attached there can be no velocity component normal to the bottom surface '***A-I***'. These two conditions can be expressed as

(5) $u = 0$

and

(6) $v = 0$

where u and v are the Cartesian velocity components. In addition, the boundary layer assumption is used for pressure, viz.,

(7) $\vec{n} \bullet \nabla P = 0$

Where $\vec{n}$ is the unit normal vector. On the surfaces '***I-L***' and '***D-L***' the same conditions are used.

On surface '***C-D***' and '***A-B***' the conditions of equations (5) through equation (8) are again imposed. On surface '***B-C***' the same two conditions are imposed on the velocity components; for the pressure a specified pressure is prescribed. Finally an interface condition must be prescribed at the interface of the oxide and the virgin AlAs material and here is where the coupling occurs with the oxide concentration. The generalized interface condition analogous to that used by Deal and Groves is specified as

(8) $\vec{V} = \frac{\rho' k_s}{N_1} C_0 \vec{n}$

where ρ' represents the density ratio of the oxide to the virgin material densities and k_s is a transfer coefficient (sometimes called the coefficient of reaction) and N_1 is the particle density of the oxidant molecules per unit volume of the oxide, a know value. C_0 is the concentration at the interface, hence Equation 8 provides the coupling between the conservation of mass and Navier-Stokes equations and the concentration

equation. It is to be noted that Equation 8 is a vector and thus provides boundary conditions for both u and v velocity components.

The concentration equation is somewhat different from the other governing equations as it is valid only in the oxide sub-region. In all other areas the concentration is zero. Thus boundary conditions must be prescribed only on surfaces '***B-F***', '***F-G***', '***C-G***' and '***B-C***'. On surfaces '***B-F***' and '***C-G***' a symmetry or no flux condition is imposed, viz.,

$$(9) \qquad \vec{n} \bullet \nabla C = 0$$

On surface '***F-G***' the generalized version of the boundary condition used by Deal and Groves is imposed.

$$(10) \qquad \vec{n} \bullet \nabla C = k_s C_0$$

On surface '***B-C***' a transfer relationship of the form

$$(11) \qquad -\vec{n} \bullet D \nabla C = h\left(C^* - C\right)$$

is imposed where C^* is the equilibrium concentration at the '***B-C***' interface.

The above equations and boundary conditions represent the system of governing equations and boundary and interface conditions that describe the physics of the problem of interest. It should be noticed that the concentration only depends on the governing diffusion equation and a prescribed geometry, while the conservation of mass and the Navier-Stokes equations are coupled to the concentration through the interface Equation (8). Thus the coupling can be considered to be one way only – from concentration to the fluid dynamics and not vice versa. This will be use to simplify the solution of the system of governing equations.

Incompressible Flow Considerations

One of the most difficult problems associated with the above equations is that the conservation of mass and the Navier-Stokes equations are numerically very complicated. This is due to the fact that when the flow is incompressible the governing equations become very 'stiff' and hence difficult to converge. Basically at very

low Mach numbers the solution matrix becomes ill-conditioned leading to slow or non-convergence and, perhaps, to loss of accuracy. There are several techniques that have been developed over the last two decades to address this problem. All utilize iterative techniques. In this study the technique of Chorin [5] was chosen because of its ability to obtain converged solutions and the experience that SRA personnel have with this technique. With this approach density, ρ, is replaced by the pressure coefficient, c_P as a dependent variable. The conservation of mass and Navier-Stokes equations are recast in the form

$$\alpha \frac{\partial\left(\frac{\rho c_P}{2}\right)}{\partial t} + \nabla \cdot \rho \vec{V} = \mathbf{0} \qquad (12)$$

and

$$\frac{\partial \rho \vec{V}}{\partial t} = -\frac{1}{2}\rho_\infty U_\infty^2 \nabla c_p - \nabla \cdot \rho \vec{V}\vec{V} + \nabla \cdot \tau \qquad (13)$$

where α is an arbitrary constant and the pressure coefficient, c_P, is defined by

$$c_p = \frac{P - P_\infty}{\frac{1}{2}\rho_\infty U_\infty^2} \qquad (14)$$

where the subscript '∞' refers to some reference condition. Equation (14) is identical to Equation (2) except for the transformation of dependent variables. Equation (13) will reduce to Equation (1) when a converged solution is obtained and the density is constant, viz.,

$$\nabla \bullet \vec{V} = 0 \qquad (15)$$

The advantage is that Equation (12) will yield converged solutions for incompressible flows whereas Equation (1) will not. The factor α is critical to the rate at which a converged solution can be obtained and 'incorrect' values can lead to divergence.

Overall Solution Technique

Because of the use of the technique of Chorin to obtain converged solutions for the fluid mechanics, it is impossible to obtain one continuous time-dependent solution to all the governing equations. Instead the technique employed is to obtain a series of converged solutions with the physical geometry of the overall device being updated after each converged solution. In this manner a series of solutions similar to a series of snapshots is obtained to describe the physics of the device. Since the concentration equation and associated boundary and interface conditions are not coupled to the conservation of mass and Navier-Stokes equations, the solution technique first obtains a solution to the concentration equation. Then a converged solution for velocity field is obtained from the method of Chorin. Once the new velocity field is obtained the geometry (or grid) associated with the four sub-regions of the device can be calculated and the above procedure repeated to follow the time dependent solution of the device. The updating of the device geometry is done through the application of the equation

$$(16) \qquad \vec{X}(t+dt) = \vec{X}(t) + \int \vec{V}(t)dt$$

where dt is an arbitrary time step chosen small enough to give a time accurate solution. The vector $\vec{X} = x\vec{i} + y\vec{j}$ where x and y are the Cartesian position coordinates. If this technique is applied directly in many cases problems will arise where coordinate lines can cross over each other after a period of time thus yielding negative geometric Jacobians. To prevent this from happening a technique that only applied Equation (16) along certain lines was developed. Looking at figure 1 it can easily be seen that there are certain key lines that outline the skeleton of the structure. If these lines are prescribed, a new coordinate system, which in general will be non-orthogonal, can be generated and the overall solution can proceed. Note that this is possible because we are obtaining a series of converged solutions to describe our time dependent process. Again looking at figure 1, it can be seen that the key skeleton lines are those that describe the outer boundary of the device and the lines that describe the interfaces between the four separate sub-regions. Once Equation (16) is applied to these lines a new geometric description of these lines is known at time $t+dt$ given the distribution know at time t. The grid point description that defines these key lines can then be

modified to obtain a smooth distribution of points on these new lines. Having accomplished this, one is now free to describe the new geometric representation of the four sub-regions. A necessary condition is that the grid points on common lines between sub-regions must be the coincident. A commonly used technique that does this is the so-call transfinite-interpolation mapping procedure (also known as Coon's patches). This technique works in one, two or three dimensions. For two dimensions, this technique uses Hermite interpolation between the four specified curves that defines each of our four sub-regions. This technique tends to give a normal grid in regions adjacent to the four specified curves of each sub-region thus yielding approximate first derivative continuity between the sub-regions, a very desirable characteristic of any grid.

Previous Results

Previously, qualitatively correct results had been obtained by just solving the diffusion equation. This obviously does not have the physics that one obtains by solving the conservation of mass – Navier-Stokes equations. When one solves the diffusion equation several assumptions must be made. First it is assumed that there is no transverse motion of the oxide layer. Secondly an assumption has to be made about the upstream later motion, viz., that the upstream lateral velocity, $\vec{W}$, is related to the velocity at the oxide-virgin material interface, $\vec{V}$, through the relationship

$$\vec{W} = (\rho' - 1)\vec{V} \tag{17}$$

where only the lateral velocity component is considered. When this calculation was performed the results shown in figure 2 resulted. The figure 2 results show a 'pencil-like' interface, confined to the AlAs region. The calculations were performed with time accurate transients and permit a determination of the growth times. It is worthwhile noting that the measurements of [3] show similar characteristics, see figure 3.

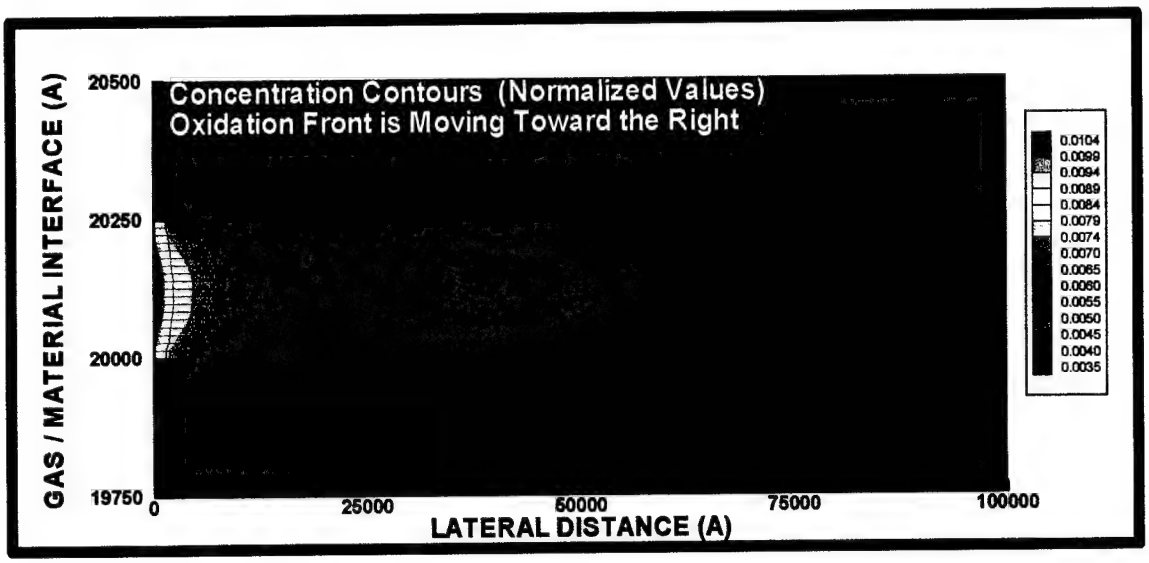

Figure 2. Oxidation contours within the AlAs layer, through solutions to the diffusion equation.

FIG. 4. TEM micrograph of the oxide tip (dark region) of an 100 Å AlAs layer oxidized at 450 °C for 80 min.

Figure 3. TEM micrograph of an oxide tip. From reference [3].

Results

To test out the solution procedure outlined above a test case was considered. Again referring to figure 1, the test case consists of a pedestal-cap sandwich surrounding an AlAs virgin material. The device chosen has the following dimensions:

(1) Line ***A-I*** = 1,000,000 Angstroms

(2) Line ***A-B*** = 20,000 Angstroms

(3) Line ***B-C*** = 500 Angstroms

(4) Line ***C-D*** = 9,500 Angstroms

(5) Line ***B-F*** = 4,000 Angstroms – Initial condition

A Cartesian grid was generated consisting of 100 grid points in the x direction and 70 grid points in the y direction. Location B (figure 1) was at grid point 31y and location C was at grid point 49y. Locations E, F, G and H were at grid point location 25x. The grid point locations of all these points remained constant as the geometry was moved, i.e., the number of grids point in each of the sub-regions remained constant throughout the computation. The distribution of grid points was chosen in a manner such that larger numbers of grid points would be concentrated in regions where large gradients of dependent variable could be expected. This is done by non-uniformly distributing grid points along the skeleton lines previously described. Thus grid points were concentrated in the regions of the pedestal-oxide and cap-oxide boundaries and the oxide-virgin material interface.

The model case had the following computational parameters:

(1) Virgin material density - $\rho = 1.0 gm/cm^3$

(2) Mass transfer coefficient – $h = 1.13x10^4 m/\sec$

(3) Coefficient of reaction – $k_s = 0.1 m/\sec$

(4) Diffusion coefficient – $D = 8.64x10^{-2} m^2/\sec$

(5) Viscosity - $\mu = 8.64x10^{-5} kg/m - \sec$

(6) Equilibrium Concentration – $C^* = 4.29x10^{22}/cm^3$

These coefficients represent the parameters that uniquely define our problem. U_∞, P_∞ and ℓ_∞ (the reference velocity, pressure and length) were chosen as 1000 Å/sec, 1 atmosphere and 1000 Å respectively. The ratio of the density of the virgin semi-conductor material to the oxide density, ρ', was initially chosen at 1.25, this variable being required for the imposition of the interface equation, Equation (8). This ratio will result in both the interface boundary between the oxide and the virgin

material moving in the positive x direction. In addition the upstream surface A-B-C-D will also be displaced in the positive x direction (see figure 1). A value of ρ' less than 1.0 will result in the upstream surface being displaced in the negative x direction.

The initial task in setting up a run is to determine a choice of inner or iteration time steps that will result in rapid accurate convergence of the diffusion equation and the conservation of mass – Navier-Stokes equations. The choice of the α parameter in the conservation of mass, as explained before, is critical. Since we were only interested in obtaining a series of converged solutions the inner or iteration time steps selected have no physical meaning. This was easily accomplished and it was found that initially that converged solutions to the diffusion equation for oxide concentration and the conservation of mass – Navier-Stokes equations could be accomplished in 250 time or iteration steps. In both cases the initial residuals (or imbalance in the initial guess for the solution) were decreased by approximately five to six orders of magnitude. It was found that converged solutions could be obtained even if the combinations of the iteration time step and the value of α were changed as much as an order of magnitude. Of course, the rates of convergence for the governing equations were slower than before. Having determined 'optimum' iteration parameters, the technique was then advanced in time to calculate the development of the oxide layer and the overall geometry of our device.

Initially this test case was run with slip conditions on Surfaces D-L, C-D and A-B. Slip conditions were also used on the oxide surface B-C. This case was run for 120 seconds. When the results of this run were plotted, it was noticed that the oxide layer sub-region was moving into the initial virgin material sub-region as expected. However the left-hand boundary of the oxide sub-region was also moving in the right direction at approximately the same rate as the oxide layer was moving into the virgin material. This is an unphysical. To prevent the above phenomenon from occurring the boundary conditions were changed to the conditions described in Equation (5) through Equation (7).

The same test case (except in this case the initial oxide layer thickness was chosen as 500 Angstroms) was then run again for 240 seconds. The results of the ox-

ide region is shown in figure (4) corresponding to time = 120 seconds. The contours extend to 10% of the peak value and display a blunter edge than that of figure 2 which showed results for solutions to the diffusion equation. There is a negligible concentration beyond this region (<10%) but it extends well beyond the AlAs, as shown by the outlines of the oxide layer displayed in figure 5. The area of rapid transverse growth is in a region where the concentration level is relatively small. In fact the concentration level at the oxide virgin material interface is about 0.02. We are currently investigating this result to determine it's significance (if any!). The horizontal lines are a reference and correspond to the initial oxide thickness of 500 Angstroms. The oxide layer initially grows at a relatively rapid rate and then with time the growth rate decreases considerably. At time = 240 seconds the oxide layer has not changed much from the results at time = 120 seconds. This is due to the fact that the boundary condition (Equation 8) determines the growth rate. Since as the oxide layer grows, the solution to the diffusion equation (Equation 4) yields smaller and smaller values of the concentration. Thus the growth rate decreases as the size of the oxide sub-region becomes larger. The shape of the oxide region shown in these figures shows the effect of solving the conservation of mass Navier-Stokes equations. Unlike the Deal and Groves solution, the oxide layer can actually push aside or be pushed aside by the pedestal and cap. It is seen here that at all times there is a pinching in the center of the oxide layer, i.e., the pedestal and cap squeeze the oxide layer. At the far right hand side of the oxide the oxide pushes out into both the pedestal and cap. It should also be noted that the effect of the large pedestal and relative thin cap are not symmetric, i.e., if a horizontal line were drawn through y = 20,250 Angstroms the solution is not symmetric about this line. This is to be expected when the conservation – Navier-Stokes equations are solved.

To further investigate this problem another test case was run. In this case, a device was chosen where the density ratio, ρ', was very close to unity, viz., 1.005. Additionally, the initial transverse dimension thickness of the oxide layer was chosen as 250 Angstroms not 500 Angstrom as in the previous case. Because of the small value of ρ' the oxide layer grows very slowly even though the value of the concentration at the oxide virgin material interface has a normalized value of approximately 0.8

after a time of 180 seconds. As can be seen from figure 6 the large transverse divergent section that was seen in the $\rho' = 1.25$ case is not nearly as exaggerated. There is some thinning of the oxide in the region of a lateral distance of 5000 Angstroms, but again not nearly as much as was exhibited in the previous case. The lack of symmetry about the value of y = 20,125 Angstroms can be seen, but it also is less exaggerated.

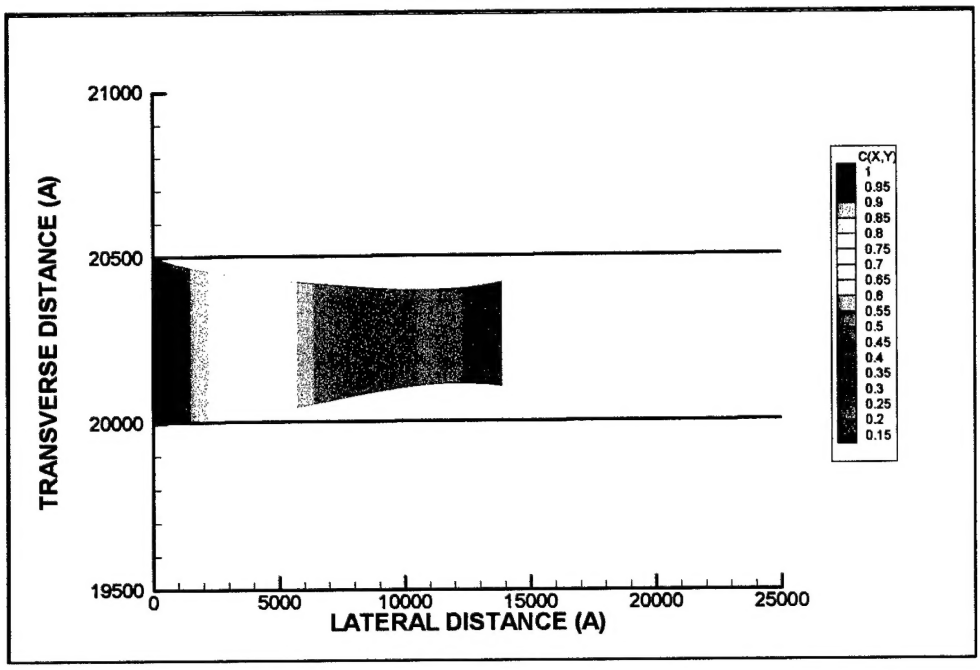

Figure 4. Oxidation contours (from 10% to 100%) within the AlAs layer, through solutions to the diffusion and Navier-Stokes equations for a density ratio of 1.25. The physical time for this profile is 120 sec.

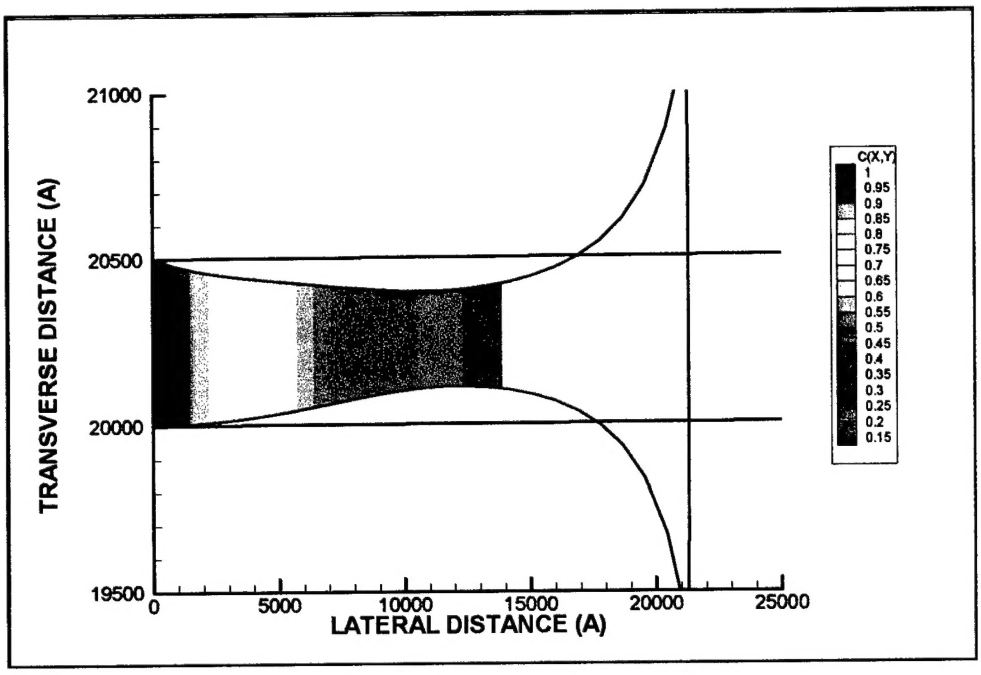

Figure 5. As in figure 4, with the addition of an outline of the oxidation region. The region to the right of that shown in figure 4, has a concentration < 10% of the peak concentration.

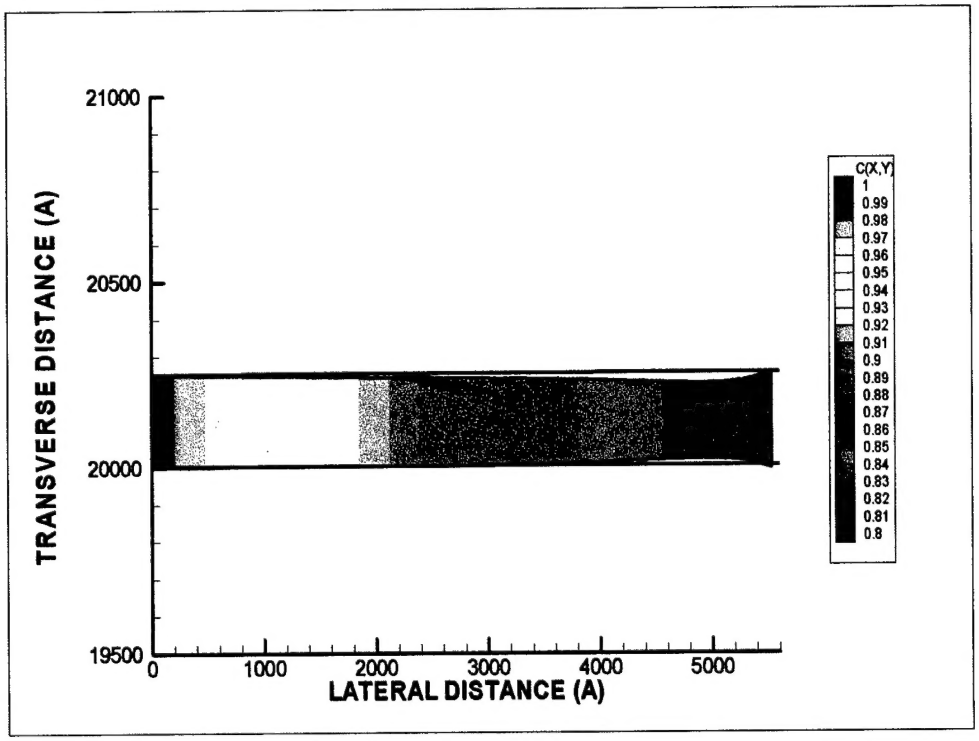

Figure 6. Oxidation contours with the AlAs layer (from 80% to 100%), through solutions tothe diffusion and Navier-Stokes equations, for a density ratio of 1.005. The physical time for this profile is 180 sec.

Conclusions

In looking at the literature the two primary sources for two-dimensional calculations that were found were Chin et. al [6]and Poncet [7]. Both of these investigators essentially solve the same set of governing equations. Chin solved a similar problem to that addressed above, but the computational domain was limited to the oxide only. No calculation was performed in either the virgin material or the mask. Poncet's problem is somewhat different and he does solve the governing equations in two separate regions. However he does not solve the governing equations in the virgin material and in the masks. Thus neither of the investigators concerns themselves with the coupled interface problem between the oxide and virgin material that was attempted in our study. The SRA study in that sense is much more ambitious. It has demonstrated that the pedestal and the cap do have an influence on the physics of the computation and they can have a significant effect on the shape of the oxide sub-region.

Earlier computations solving only the diffusion equation, figure 2, were encouraging in that they qualitatively predicted the shape of the oxide region. A blunter, but tapered shape was found for one set of parameters, and a blunt shape without tapering was found for another set of parameters. While a complete parametric study has not been undertaken the results do demonstrate the interaction of the cap and the pedestal with the oxide region, and suggest that additional source terms are needed in the interface to model the effects that occur between these regions.

In general, a numerical procedure that solves the coupled system of partial differential equations the growth of an oxide layer into a semi-conductor material has been developed. The numerical procedure allows for a variety boundary equation and allows for the overwriting of the governing equations in internal interface surfaces. Solutions have been obtained for a variety of cases.

References

1. Deal, B.E. and A.S. Grove, *General relationship for the thermal oxidation of silicon.* Journal of Applied Physics, 1965. **36**(12).
2. Ochiai, M., et al., *Kinetics of thermal oxidation of AlAs in water vapor.* Applied Physics Letters, 1996. **68**(14): p. 1898-1900.
3. Naone, R.L. and L.A. Caldren, *Surface energy model for the thickness dependence of the lateral oxidation of AlAs.* Journal of Applied Physics, 1997. **82**(5): p. 2277-2280.
4. Yoshikawa, T., et al., *Self-stopping selective-oxidation process of AlAs.* Applied Physics Letters, 1998. **72**(18): p. 2310-2312.
5. Chorin, A.J., *A Numerical Method for Solving Incompressible Viscous Flow Problems.* Journal of Computational Physics, 1967. **2**: p. 12-16.
6. Chin, D., et al., *Two-dimensional Oxidation.* IEEE Transactions on Electron Devices, 1983. **ED-30**(7): p. 744-749.
7. Poncet, A., *Finite-element simulation of local oxidation of Silicon.* IEEE Transactions on Computer Aided Design, 1985. **CAD-4**(1): p. 41-53.